Nonisothermal Crystallization, Melting Behavior, and Morphology of Polypropylene/Linear Bimodal Polyethylene Blends

Jianglei Qin, Jungang Gao, Zhiting Li, Mingtao Run

College of Chemistry and Environmental Science, Hebei University, Baoding 071002, China

Received 12 October 2006; accepted 22 July 2007
DOI 10.1002/app.27157
Published online 9 October 2007 in Wiley InterScience (www.interscience.wiley.com).

ABSTRACT: The nonisothermal crystallization, melting behavior, and morphology of isotactic polypropylene (PP)/linear bimodal polyethylene (LBPE) blends were studied with differential scanning calorimetry, scanning electron microscopy, and polarized optical microscopy. The results showed that PP and LBPE were miscible to a certain extent, and there was no obvious phase separation in the blends. The modified Avrami analysis, Ozawa equation, and Mo method were used to analyze the nonisothermal crystallization kinetics of the blends. The values of the Avrami exponent indicated that the crystallization nucleation of the blends was homogeneous, the growth of spherulites was three-dimensional, and the crystallization mechanism of PP was not affected much by LBPE. The crystallization activation energy was estimated by the Kissinger method. The results obtained with the modified Avrami analysis, Mo method, and Kissinger method agreed well. The addition of a minor LBPE phase favored an increase in the overall crystallization rate of PP, showing some dilution effect of LBPE on PP. The PP spherulites decreased obviously with increasing content of LBPE. © 2007 Wiley Periodicals, Inc. J Appl Polym Sci 107: 1235–1242, 2008

Key words: activation energy; blends; crystallization; melt; morphology

INTRODUCTION

Polypropylene (PP) is one of the most widely used polyolefin materials, but its applications in some fields are limited by its low fracture toughness at low temperatures and high notch sensitivity at room temperature. Compounding PP with a dispersed elastomeric phase [e.g., ethylene–propylene–diene rubber (EPDM)] is widely practiced[1–5] because the rubber can increase the overall toughness of the PP matrix.[6] However, the addition of elastomers often has negative effects on some properties of PP, such as stiffness, hardness, and rheological properties.[7]

The development of metallocene catalysts has led to the production of numerous new polyolefin materials, among which linear bimodal polyethylene (LBPE) is extremely attractive. There are high-molecular-weight and low-molecular-weight components simultaneously in the LBPE matrix, and the low-molecular-weight component gives it good rheological properties, and the mechanical properties are well maintained.[8] Because of its good mechanical properties, thermal stability, and aging resistance in comparison with conventional EPDM, an metatocine-catalyzed polyethylene (mPE) elastomer can impart higher impact strength as a modifier of PP.[9] Moreover, previous work has shown improved fracture behavior at low temperatures and better dynamic properties with an mPE modifier.[10] Because of its better rheological properties, LBPE-modified PP could have better rheological properties than an mPE elastomer. In addition, like mPE, LBPE is granular, and its processing technology is much better than that of other elastomers and rubbers, but the application of LBPE to the modification of PP has never reported.

It is well known that the physical properties of semicrystalline polymeric materials strongly depend on their crystallization and microstructure; thus, investigations of the crystallization behavior and morphology of polymer blends are significant both theoretically and practically. In particular, the crystallization behavior during nonisothermal crystallization from the melt is of increasing technological importance because these conditions are the closest to practical industrial conditions. Therefore, it is highly desirable to investigate the crystallization behavior and morphology to optimize the blend composition and processing technology of LBPE-modified PP. However, such detailed investigations have not been reported until now.

In this study, the melting and crystallization behavior of PP/LBPE blends was investigated, and the nonisothermal crystallization kinetics of the

Correspondence to: J. Qin (thunder20@163.com).

blends were studied with the modified Avrami analysis, Ozawa equation, and Mo method. The morphologies of the blends were also studied to investigate the effect of LBPE on the microstructure of the blends.

EXPERIMENTAL

Materials and sample preparation

The PP [type T36F, melt flow rate (230°C/2.16 kg) = 2.46 g/10 min] used in this study was a commercial polymer supplied by Qilu Petrochemical Co. (China); the LBPE [type FB2230, melt flow rate (190°C/2.16 kg) = 0.25 g/10 min] was a product of Northern European Chemical Industry (Finland).

Blend samples were prepared by melt blending in a twin-screw extruder (TE-34, Coperion Keya, Nanjing China) with a length/diameter ratio of 28, and the temperature of the extruder was around 180–220°C. The weight ratios of PP to LBPE in the blends were 100/0, 90/10, 80/20, 60/40, and 0/100.

Thermal analysis

A PerkinElmer (USA) DSC-7 apparatus was used to record the heat flow during the melting and nonisothermal crystallization processes of the blends.

All the operations were carried out under a nitrogen environment. The temperature and melting enthalpy were calibrated with standard indium. The sample weights were about 9 mg.

For the melting behavior, samples were heated from room temperature to 200°C at a rate of 10°C/min. To erase the influence of the thermal history, the temperature was held at 200°C for 3 min. Then, the samples were cooled to 30°C at various constant cooling rates: 2.5, 5, 10, and 20°C/min. A second run was carried out after the melted samples were cooled to 30°C and held for 3 min.

Morphology analysis

Scanning electron microscopy (SEM) micrographs were taken on a KYKY 2800B (KYKY Technology Development Ltd., China) microscope according to the method of Campbell and White,[11] and impact fracture surfaces were examined.

Polarized optical microscopy (POM) micrographs were obtained with an XPT-7 polarized optical microscope (Jiangnan Optical, China) equipped with an Olympus (Japan) camera. A compression-molded film was sandwiched between a microscope slide and a cover glass; then, the samples were heated from room temperature to 210°C, kept at that temperature for 5 min to allow complete melting, and then cooled to 140°C for isothermal crystallization for 1 h.

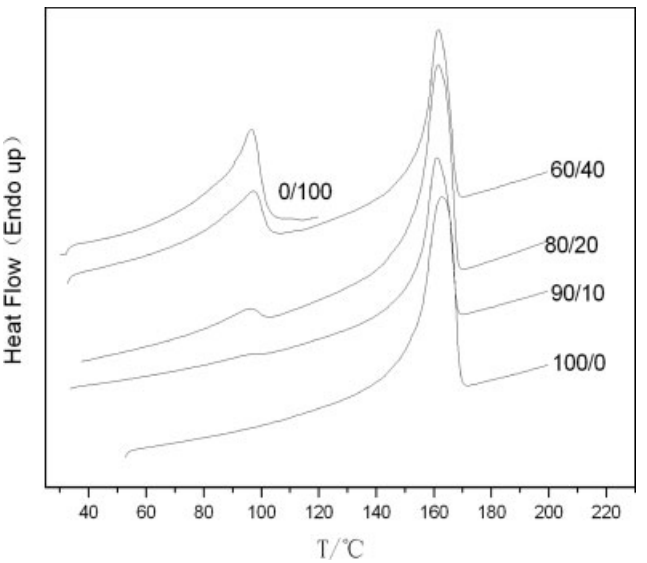

Figure 1 DSC melting curves of PP/LBPE blends at a heating rate of 10°C/min.

RESULTS AND DISCUSSION

Melting and crystallization behavior of PP/LBPE blends

Figure 1 shows the differential scanning calorimetry (DSC) melting heat flow of the pure polymers and their blends. The melting temperature of PP decreases a little with the LBPE content increasing; however, the melting temperature of LBPE increases with increasing PP content, but the differences are not obvious. This observation indicates that there is some interaction between PP and LBPE molecules, which is attributed to partial miscibility of PP and LBPE. The melting temperature of PP in the blends is between 160 and 165°C. This indicates that PP, both in the pure state and in the blends, exhibits only the α-crystal form because the melting temperature of the α-crystal form is in the range of 160–176°C.[12,13]

For the pure PP, pure LBPE, and their blends, which are crystallizable, nonisothermal crystallization was performed from the molten state by DSC with various cooling rates of 2.5–20°C/min. Figure 2 shows the crystallization exotherms for some PP/LBPE blends versus pure PP and pure LBPE (cooling rate = 10°C/min). All DSC traces show two crystallization peaks, except those of the pure polymers; this indicates that two crystallizable components exist in the blend systems. Crystallization of PP occurs much earlier than that of LBPE upon cooling. Both the PP exothermal peak and the LBPE exothermal peak move to higher temperatures, and this means that LBPE has some dilution effect on PP and PP acts as a nucleus agent while LBPE is crystallizing; this

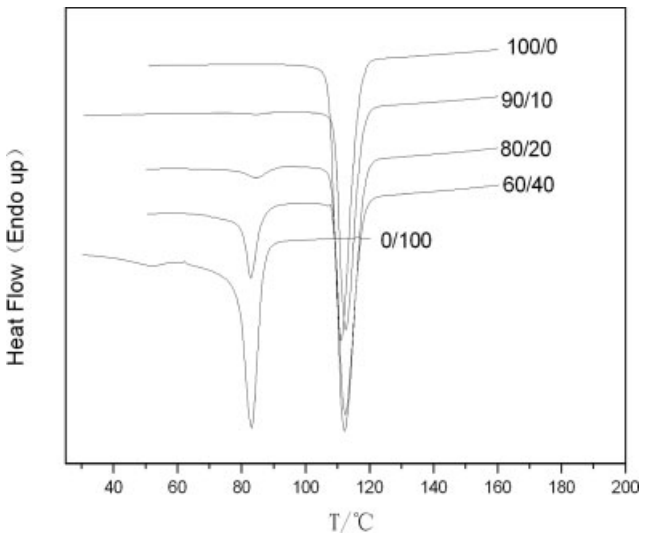

Figure 2 DSC nonisothermal crystallization curves of PP/LBPE blends at a cooling rate of 10°C/min.

change can also be seen in the crystallization rate constants.

As an example, Figure 3 shows the typical crystallization exotherms for 80/20 PP/LBPE blends at various cooling rates. The crystallization peak temperature for the pure polymers and their blends (T_{p2}) is clearly shifted to a lower temperature as the cooling rate increases (see Table I). The decrease of T_{p2} with a higher cooling rate is due to the fact that the crystallization rate is lower than the experimental cooling rate.[14] At a lower cooling rate, PP molecules have enough time to form the necessary nuclei for crystallization and, therefore, come to a higher T_{p2}, and the crystallization temperature and the crystallinity are correspondingly higher (see Table I). The crystallinity can be calculated according to the literature,[15] and the values are listed in Table I. From Table I, we can see that the crystallinity of 80/20 PP/LBPE is much higher than that of pure PP because some LBPE molecules have entered the PP crystal. However, the crystallinity of 60/40 PP/LBPE is a little lower than that of pure PP because some PP chains have dissolved into the LBPE melt.

Nonisothermal crystallization kinetics

Up to now, several analytical methods have been developed to describe the nonisothermal crystallization kinetics of polymers: (1) the modified Avrami analysis,[16–18] (2) the Ozawa equation,[19,20] (3) the Ziabicki analysis,[21,22] and (4) others[23–26] such as the Mo method. In this article, the modified Avrami analysis and Mo method are applied to describe the nonisothermal crystallization kinetics of PP/LBPE blends, and a contrastive study is performed.

The Avrami analysis[18,27,28] has been widely used to describe the isothermal crystallization kinetics of polymers:

$$1 - X_t = \exp(-kt^n) \tag{1}$$

where X_t is the relative crystallinity, k is the crystallization rate constant, and n is the Avrami exponent. Here, the value of n depends on the nucleation mechanism and growth dimensions, and parameter k is a function of the nucleation and growth rate. X_t as a function of the crystallization time is defined as follows:

$$X_t = \frac{\int_{t_0}^{t}(dH_C/dt)dt}{\int_{t_0}^{t_\infty}(dH_C/dt)dt} \tag{2}$$

where dHc/dt is the rate of heat evolution and t_0 and t_∞ are the times at which crystallization starts and ends, respectively.

The Avrami equation can be modified to describe nonisothermal crystallization.[16,17,29,30] For nonisothermal crystallization at a chosen cooling rate, X_t is a function of crystallization temperature T. That is, eq. (2) can be rewritten as follows:

$$X_t = \frac{\int_{T_0}^{T}(dH_C/dT)dT}{\int_{T_0}^{T_\infty}(dH_C/dT)dT} \tag{3}$$

where T_0 and T_∞ represent the onset and end temperatures of crystallization, respectively.

As an example, Figure 4 shows the relative crystallinity of PP in 80/20 PP/LBPE blends at various cooling rates. All curves in Figure 4 show a reversed sigmoidal shape, indicating a fast primary process

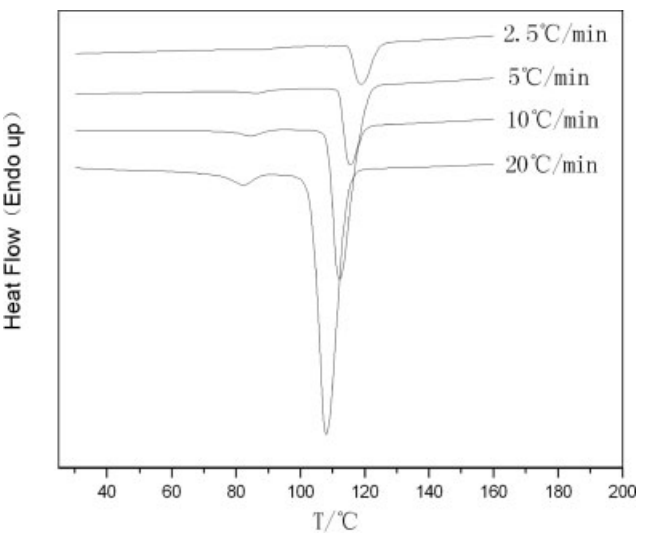

Figure 3 DSC nonisothermal crystallization curves of PP in 80/20 PP/LBPE blends at various cooling rates.

TABLE I
Melting Behaviors and Nonisothermal Crystallization Parameters of PP/LBPE Blends at Different Values of *D* on the Basis of Avrami Analysis

Sample (PP/LBPE)	D (°C/min)	n	ln k'	$t_{1/2}$ (min)	T_p (°C)	ΔH_{pp} (J/g)	Crystallinity (%)
100/0	2.5	5.33	−7.69	3.96	118.6	88.4	47.1
	5.0	5.05	−4.06	3.23	115.1	87.5	46.6
	10	4.99	−0.93	1.76	111.0	86.6	46.1
	20	4.51	2.18	0.91	106.0	83.8	44.6
80/20	2.5	4.59	−6.50	3.80	119.1	76.3	50.8
	5.0	4.23	−2.97	1.86	115.6	75.5	50.3
	10	4.56	−0.46	1.02	112.1	74.4	49.5
	20	4.25	2.41	0.52	108.1	72.1	48.0
60/40	2.5	4.92	−6.31	3.36	119.1	52.5	46.6
	5.0	4.80	−3.13	1.78	115.7	52.1	46.3
	10	4.88	−0.31	1.00	112.4	50.6	44.9
	20	4.53	2.43	0.54	108.1	49.3	43.8

during the initial stage and a slower secondary process during the later stage. The plot of X_t versus T shifts to the low temperature region as the cooling rate increases, indicating that the crystallization is enhanced as the temperature decreases. That is because of the strong temperature dependence on the nucleation and growth parameters.[31] After the maximum in the heat flow curves has passed, a small fraction of crystallinity develops by slower, secondary kinetic processes. The lower cooling rate provides more fluidity, more diffusivity, and more time at a high temperature for perfect crystallization because of the lower relative viscosity, thus inducing much higher crystallinity at lower cooling rates than that at higher cooling rates, as shown in Table I.

Crystallization temperature T can be converted to crystallization time t with the following equation[22,29]

$$t = \frac{T_0 - T}{D} \tag{4}$$

where D is the cooling rate. With eq. (4), the temperature axis in Figure 4 can be transformed into a timescale, as shown in Figure 5. The sigmoidal shape of the curves suggests that the modified Avrami analysis is applicable to the nonisothermal crystallization of PP/LBPE blends. Meanwhile, the crystallization half-time ($t_{1/2}$) can be calculated directly from the plot of the relative crystallinity versus time,[18,32] as shown in Table I.

Equation (1) can be rewritten in a double-logarithm form:

$$\ln[-\ln(1 - X_t)] = \ln(-k) + n\ln(t) \tag{5}$$

Then, the Avrami parameters can be estimated from $\ln[-\ln(1 - X_t)]$ versus $\ln t$. Here, the crystallization rate of nonisothermal crystallization depends on the cooling rate. Thus, k should be corrected adequately.

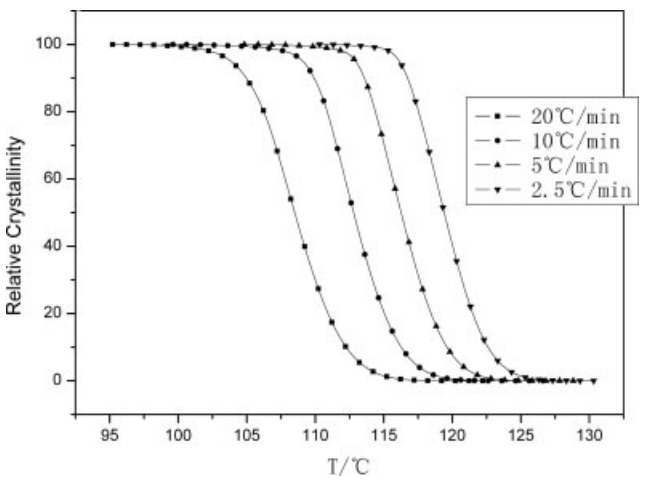

Figure 4 Plot of X_t versus T for PP in 80/20 PP/LBPE blends for nonisothermal crystallization at various cooling rates.

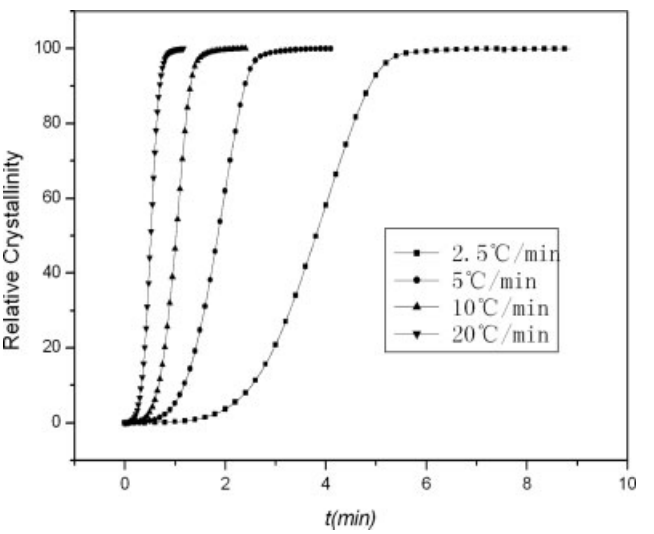

Figure 5 Relationship of X_t versus t for PP in 80/20 PP/LBPE blends for nonisothermal crystallization at various cooling rates.

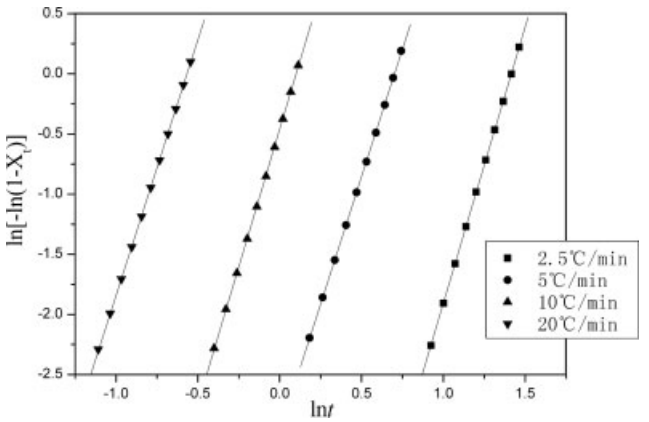

Figure 6 Avrami plot for PP in 80/20 PP/LBPE blends for nonisothermal crystallization at various cooling rates.

Assuming a constant cooling rate, the crystallization rate constant can be corrected as follows:[29] $\ln k' = \ln k/D$.

Figure 6 shows the plot of $\ln[-\ln(1 - X_t)]$ versus $\ln t$ for the nonisothermal crystallization of 80/20 PP/LBPE blends. All lines in Figure 6 are almost parallel to one another, shifting to less time with an increasing cooling rate. This implies that the nucleation mechanism and crystal growth geometries are similar, although the cooling rates are different. The Avrami parameters were estimated from the plot of $\ln[-\ln(1 - X_t)]$ versus $\ln t$, and the values are listed in Table I. Regardless of the cooling rates, n for pure PP is in the range of 4.51–5.33, showing the homogeneous nucleation mechanism of PP, but n calculated from nonisothermal kinetics cannot be compared to that of isothermal kinetics. The n values of PP/LBPE blends are smaller (4.25–4.9.5) than those of pure PP, showing a small heterogeneous nucleation effect of LBPE on the PP matrix.

However, the crystallization rate is dependent on the blend composition and cooling rates. On the one hand, for pure PP, the crystallization rate constant (k') increases with increasing cooling rate, whereas $t_{1/2}$ decreases with increasing cooling rate (see Table I). Similar trends in both k' and $t_{1/2}$ can be observed for the 80/20 and 60/40 PP/LBPE blends. On the other hand, both k' and $t_{1/2}$ are also influenced by the addition of LBPE; that is, at the same cooling rate, k' slightly increases with the LBPE content increasing, and $t_{1/2}$ is adversely affected. Thus, the crystallization rate is accelerated with the introduction of LBPE in PP, and this is due to the fact that LBPE acts as a diluent and nucleation agent at higher temperatures, and then the mobility of PP molecules in the blends is increased compared to that in pure PP; the higher mobility of PP molecules facilitates the transport of PP molecules from the melt to the growing crystals, and so the crystallization rate increases. Meanwhile, the tacticity and flexibility of LBPE molecules are high, and the high mobility of LBPE molecules helps PP molecules to transit to the growing crystal; because of the interaction of PP and LBPE molecules, some LBPE molecules enter the PP crystal and then come to a higher crystallinity (see Table I). The crystallinity of 60/40 PP/LBPE blends is lower than that of pure PP because too much LBPE content in the blends completely destroys the PP spherulites (see the POM photographs) and/or crystals and dissolves some PP.

The Ozawa equation is another important theory for nonisothermal crystallization kinetics and is expressed as follows:

$$1 - C(T) = \exp[-K(T)/D^m] \tag{6}$$

where $C(T)$ is the relative crystallinity at given temperature T, $K(T)$ is the growth rate constant, and m is the Ozawa exponent. According to the Ozawa equation, we can get a plot of $C(T)$ versus D (see Fig. 7). From Figure 7, we see that we cannot get straight lines because the differences between the cooling rates are too high.[33]

For comparison, a new simple method, proposed by Mo et al.,[23] is expressed as follows:

$$\ln D = \ln F(T) - a \ln t \tag{7}$$

where $F(T) = [K(T)/k]^{1/m}$ refers to the cooling rate value, which must be chosen within the unit of crystallization time when the measured system amounts to a certain relative crystallinity. Then, the $F(T)$ value has a definite physical and practical meaning; that is, at a certain relative crystallinity, a high value of $F(T)$ means that a high cooling rate is needed to reach this X_t value in a unit of time, which reflects

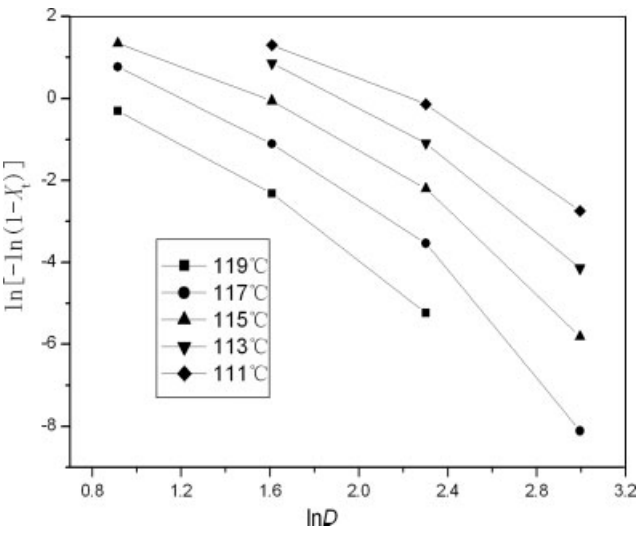

Figure 7 Plots of $\ln[-\ln(1 - X_t)]$ versus $\ln D$ for the nonisothermal crystallization of PP at various temperatures on the basis of the Ozawa analysis.

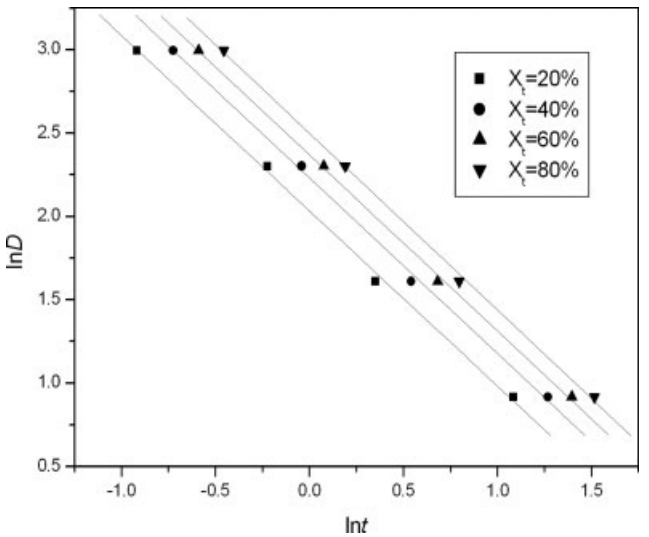

Figure 8 Mo plot for PP in 80/20 PP/LBPE blends for nonisothermal crystallization at different values of X_t.

the difficulty of its crystallization process. a is the ratio of n to m ($a = n/m$). According to eq. (7), $F(T)$ and a can be determined from the slope and intercept, respectively, of a plot of the logarithm of the cooling rate versus the logarithm of time at different values of X_t. Figure 8 presents the results for 80/20 PP/LBPE blends according to eq. (7) at relative crystallinities of 20, 40, 60, and 80%. The values of $F(T)$ and a for all the samples are listed in Table II. The $F(T)$ values increase with increasing relative crystallinity for the same blends. The values of a are almost a constant for a given composition at different relative crystallinities, and this indicates that the new method is successful at describing the nonisothermal crystallization process of PP/LBPE blends. However, at the same relative crystallinity, the $F(T)$ values of PP are higher than those of PP/LBPE blends, showing that a high cooling rate is needed to get a certain relative crystallinity within a unit of crystallization time and implying that the crystallization rate of PP is lower than that of PP/LBPE blends. As for pure PP, the a values are near 1, showing that m matches n, but that of the PP/LBPE blends is not the same because of the addition of LBPE; this is another proof that LBPE affects the crystallization behavior of PP. There are some differences between n and m because n does not take the cooling rate into account.

TABLE II
Nonisothermal Crystallization Parameters of PP/LBPE Blends with Different Values of X_t on the Basis of Mo Analysis

Sample (PP/LBPE)	X_t (%)	ln $F(T)$	a	E_a (kJ/mol)
100/0	20	2.153	1.059	−228. 8
	40	2.332	1.066	
	60	2.467	1.087	
	80	2.606	1.117	
80/20	20	2.034	1.052	−242.2
	40	2.232	1.054	
	60	2.370	1.055	
	80	2.500	1.061	
60/40	20	2.019	1.130	−242.7
	40	2.216	1.138	
	60	2.351	1.150	
	80	2.483	1.162	

For nonisothermal crystallization, the crystallization activation energy (E_a) can be estimated from the variation of the crystallization peak temperature (T_p) with D by the Kissinger approach:[34]

$$\frac{d[\ln(D/T_p^2)]}{d(1/T_p)} = -\frac{E_a}{R} \tag{8}$$

where d is the differential coefficient and R is the universal gas constant.

The Kissinger plot, that is, the plot of $\ln(D/T_p^2)$ versus $1/T_p$, is shown for PP/LBPE blends in Figure 9. E_a is estimated to be −228. 8 kJ/mol for pure PP, −242.2 kJ/mol for 80/20 PP/LBPE blends, and −242.7 kJ/mol for 60/40 PP/LBPE blends (see Table II). In comparison, E_a of pure PP is higher than that of the PP/LBPE blends. From the perspective of kinetics, the activation energy can be correlated to the crystallization rate. The crystallization rate constants obtained from Avrami analysis decrease in the order of 60/40 PP/LBPE blends ≈ 80/20 PP/LBPE blends > PP, and the difference between the two blend systems is negligible; the crystallization rate constants obtained from the Mo method and Kissinger equation decrease in the same order of 60/40 PP/LBPE blends ≈ 80/20 PP/LBPE blends > PP, so

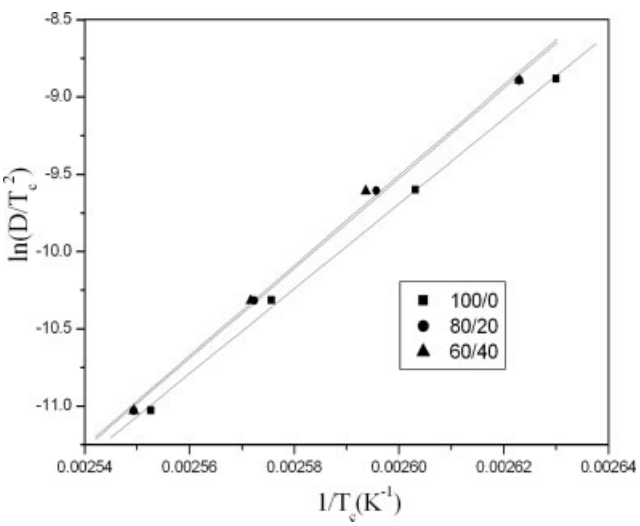

Figure 9 Kissinger plot of $\ln(D/T_p^2)$ versus $1/T_p$ of PP/LBPE blends for nonisothermal crystallization with different LBPE contents.

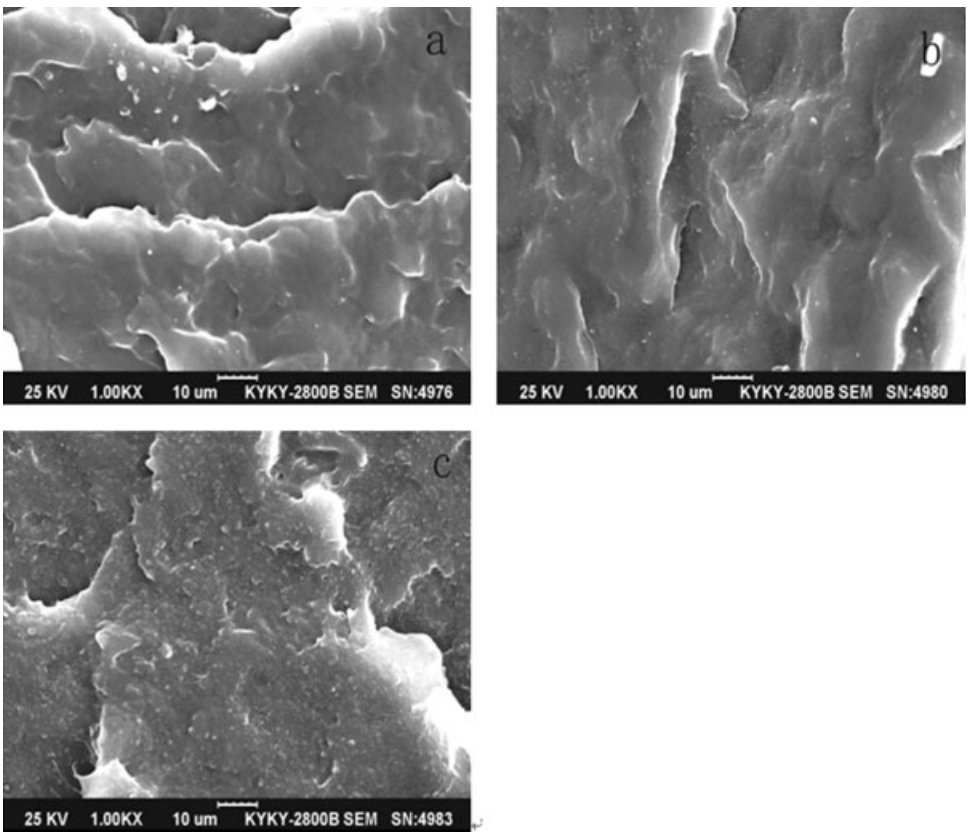

Figure 10 SEM micrographs of PP/LBPE blends: (a) 100/0, (b) 80/20, and (c) 60/40.

the conclusions derived from the three methods agree well.

Morphology analysis

It is well known that the properties of materials greatly depend on their morphological structure. For polymer blends or composites, the dispersion of the components is extremely important. A series of SEM micrographs of the impact fracture surfaces obtained during notch impact testing of PP/LBPE blends are shown in Figure 10 and demonstrate clearly that LBPE is uniformly dispersed in the PP matrix. Pure PP [Fig. 10(a)] has a relatively smooth surface and exhibits typically brittle fracture behavior. A similar appearance can be observed on the fractured surface of the 80/20 PP/LBPE blends [Fig. 10(b)]; because there is not enough LBPE content, it can be still characterized as brittle fracture, with a few LBPE particles dispersed in the matrix. With the content of LBPE increasing to 60/40 PP/LBPE [Fig. 10(c)], the fracture surface is accompanied by obvious plastic deformation, and the LBPE phase is a homogenized dispersion in the PP matrix and forms the sea–island structure. LBPE forms a dispersed phase, and the dimensions depend on the blend composition. In the 80/20 PP/LBPE blends, the dimensions of the dispersed LBPE phase are rather small. When the content of LBPE is high [see Fig. 10(c)], the dimensions of the dispersed phase are obviously larger, but no obvious phase separation has been seen in the blends.

The SEM photographs seem to show that PP and LBPE are quite miscible, but DSC shows partial miscibility. The reason for this contradiction is that the impact testing samples were injected, the high shear rate in the injecting process helped LBPE to disperse into the PP matrix uniformly, and the interface of PP and LBPE became unclear.

Figure 11 shows POM micrographs of PP/LBPE blends isothermally crystallized at 140°C for 1 h. As shown in Figure 11(a), pure PP reveals a well-defined and large spherulite morphology; the spherulites grow and impinge on one another to form particular polygonal spherulites with clear boundaries. Well in the 90/10 PP/LBPE blends, the dimensions of the PP spherulites decrease, whereas the right-angled intersection is still evident and clear [see Fig. 11(b)]. When the LBPE content increases to 80/20 PP/LBPE [Fig. 11(c)], the spherulites become less perfect, the right-angled intersection becomes diffuse, the size decreases, and at the same time the spherulite boundaries disappear. When the LBPE content is up to 60/40 PP/LBPE [Fig. 11(d)], the spherulites are hardly seen, and this shows that the spherulites are entirely destroyed. Overall, the addi-

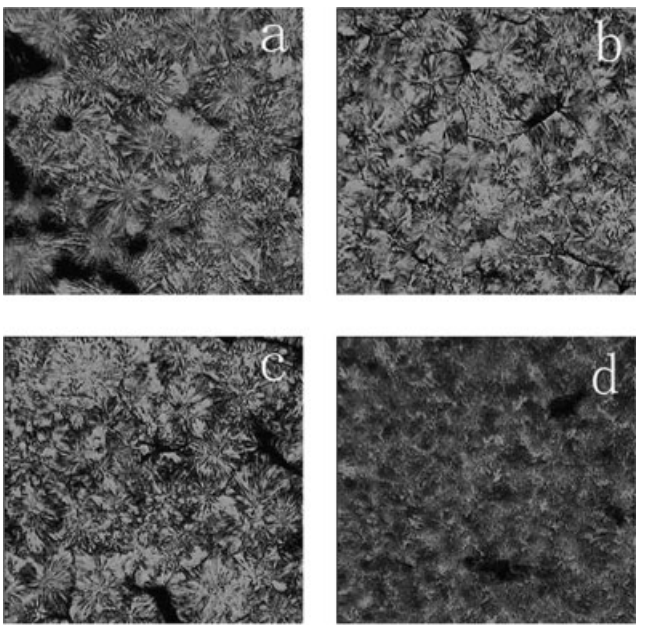

Figure 11 POM micrographs of PP/LBPE blends with 100× magnification. (a) 100/0, (b) 90/10, (c) 80/20, and (d) 60/40.

tion of LBPE greatly affects the spherulite size and morphology for PP. The spherulite size decreases, and this is due to the crystallization ability of PP being disrupted at the higher content of LBPE; PP molecular chains are more difficult to arrange in an ordered manner than those of pure PP, and this causes a large number of spherulites to grow in limited space. Therefore, the perfect spherulites cannot form at the higher content of LBPE, more crystal defects appear, and crystallinity decreases as a result.

CONCLUSIONS

PP/LBPE blends, prepared by a conventional melt-blending method, have been investigated with respect to their melting behavior, crystallization behavior, and morphology. First, the study of the melting and nonisothermal crystallization behavior shows that PP and LBPE are miscible to a certain extent. Second, the nonisothermal crystallization kinetics of the blends have been investigated fairly well by both the modified Avrami analysis and Mo method, but the Ozawa equation is not fit for this system. The results show that the nucleation mechanism of this system is homogeneous, and the crystallization mechanism of PP is not affected much by LBPE. Third, the crystallization rate is increased and the crystallization activation energy is decreased by LBPE. Fourth, the SEM observations indicate that the LBPE phase is uniformly dispersed in the PP matrix, and the dimensions of the dispersed phase increase with increasing LBPE content. The POM results suggest that the addition of LBPE results in an obvious decrease of the spherulite size and overall perfection.

References

1. Karger-Kocsis, J.; Kalló, A.; Kuleznev, V. N. Polymer 1984, 25, 279.
2. Coppola, F.; Greco, R.; Martuscelli, E.; Kammer, H. W. Polymer 1987, 28, 47.
3. Tam, W. Y.; Cheung, T.; Li, R. K. Y. Polym Test 1996, 15, 452.
4. Van der Wal, A.; Mulder, J. J.; Oderkerk, J.; Gaymans, R. J. Polymer 1998, 39, 6781.
5. Yokoma, Y.; Ricco, T. J Appl Polym Sci 1997, 66, 1007.
6. Karger-Kocsis, J. Polypropylene—Structure, Blends and Composites; Chapman & Hall: London, 1994.
7. Qiu, G. X.; Raue, F.; Ehrenstein, G. W. J Appl Polym Sci 2002, 83, 3029.
8. Gao, J.-G.; Yu, M.-S.; Li, Z.-T. Eur Polym J 2004, 44, 1533.
9. Sylvest, R. T.; Lancester, G.; Betso, S. R. Kautsch Gummi Kunstst 1997, 50, 186.
10. Raue, F.; Ehrenstein, G. W. J Elast Plast 1999, 31, 194.
11. Campbell, D.; White, J. R. Polymer Characterization; Chapman & Hall: New York, 1989.
12. Shieh, Y. T.; Lee, M. S.; Chen, S. A. Polymer 2001, 42, 4439.
13. Ha, C. S.; Kim, S. C. J Appl Polym Sci 1988, 35, 2211.
14. Park, J. Y.; Kwon, M. H.; Park, O. O. J Polym Sci Part B: Polym Phys 2000, 38, 3001.
15. Kirshenbaum, I.; Wilchinsky, Z. W.; Groten, B. J Appl Polym Sci 1964, 8, 2723.
16. Herrero, C. H.; Acosta, J. L. Polymer 1994, 26, 786.
17. De Juana, R.; Jauregui, A.; Calahora, E.; Cortazar, M. Polymer 1996, 37, 3339.
18. Lee, S. W.; Ree, M.; Park, C. E.; Jung, Y. K.; Park, C. S.; et al. Polymer 1999, 40, 7137.
19. Ozawa, T. Polymer 1971, 12, 150.
20. Ozawa, T.; Huang, H.; Gu, L.; Ozaki, Y. Polymer 2006, 47, 3935.
21. Ziabicki, A. Colloid Polym Sci 1974, 6, 252.
22. Ziabicki, A. Appl Polym Symp 1967, 6, 1.
23. Liu, T. X.; Mo, Z. S.; Wang, S. E.; Zhang, H. F. Polym Eng Sci 1997, 37, 568.
24. Caze, C.; Devaux, E.; Crespy, A.; Cavrot, J. P. Polymer 1997, 38, 497.
25. Nakamura, K.; Katayama, K.; Amano, T. J Appl Polym Sci 1973, 17, 1031.
26. Chan, T. W.; Isayev, A. I. Polym Eng Sci 1994, 34, 461.
27. Avrami, M. J Chem Phys 1939, 7, 1103.
28. Avrami, M. J Chem Phys 1940, 8, 212.
29. Jeziorny, A. Polymer 1978, 19, 1142.
30. Tobin, M. C. J Polym Sci Polym Phys Ed 1974, 12, 399.
31. Seo, Y. S.; Kim, J. H.; Kin, K. U.; Kim, Y. C. Polymer 2000, 41, 2639.
32. Xu, W. B.; Ge, M. L.; He, P. S. J Appl Polym Sci 2001, 82, 2281.
33. Ren, M.; Mo, Z.; Chen, Q. Acta Polym Sinica 2005, 3, 374.
34. Kissinger, H. E. J Res Natl Bur Stand U S A 1956, 57, 217.